

<https://doi.org/10.1038/s41698-025-01230-y>

# Prospective tumour mutation burden and neoantigen profiling predicts immunotherapy response in metastatic melanoma

Check for updates

Yizhe Mao<sup>1,2,3</sup>, Tuba N. Gide<sup>1,2,3</sup>, Nigel G. Maher<sup>1,2,3,4</sup>, Danielle Vignati<sup>1,4</sup>, Andrea Boutros<sup>1,5</sup>, Paola Cornejo-Páramo<sup>1,2,3</sup>, Alison J. Potter<sup>4</sup>, Matteo S. Carlino<sup>1,2,6</sup>, Elizabeth C. Paver<sup>1,7,8</sup>, Hazel Burke<sup>1</sup>, Alexander M. Menzies<sup>1,2,9,10</sup>, Serigne N. Lo<sup>1,2,3</sup>, Inês Pires da Silva<sup>1,2,3,11</sup>, Richard A. Scolyer<sup>1,2,3,4,12</sup>, Georgina V. Long<sup>1,2,3,9,10,12</sup>, Ismael A. Vergara<sup>1,2,3,12</sup> & James S. Wilmott<sup>1,2,3,12</sup> ✉

Tumour mutation burden (TMB) is a promising biomarker in predicting immunotherapy response, yet its reproducibility across target panels needs to be established. This study assessed the reproducibility of TMB estimates in melanoma using TruSight Oncology 500 across two laboratories and compared these results with the FoundationOne CDx and QIAseq TMB IO panels. High concordances in TMB estimation, mutation calls, and *BRAF* and *N/K/HRAS* hotspot variants were observed between platforms. In a cohort of 198 pre-treatment biopsies from patients treated with immune checkpoint inhibitors, high TMB ( $\geq 10$  mut/Mb) was associated with significantly improved response and progression-free survival (PFS), while somatic mutations in *PTPRD* and a germline variant in *PIK3CA* (I391M) were associated with favourable outcomes independent of TMB. Neoantigen profiling of 135 samples demonstrated that neoantigen load, particularly neoepitopes with strong-binding to class II MHC, had a superior predictive value over TMB for PFS. Mutations in *NF1* and *ROS1* that produce a neoantigen were also linked to improved outcomes. These results support the reproducibility of TMB estimation and highlight the added value of neoantigen profiling in predicting immunotherapy benefits in melanoma.

Immune checkpoint inhibitors (ICIs) targeting the programmed cell death protein 1 (PD-1) and cytotoxic T-lymphocyte-associated protein 4 (CTLA-4) receptors have demonstrated significant efficacy in melanoma. Single-agent anti-PD-1 and combination anti-PD-1/anti-CTLA-4 therapy have achieved long-term (10 year) melanoma-specific survival rates of 45.2% and 52%, respectively, in patients with advanced melanoma<sup>1–3</sup>. The combination of anti-PD-1/anti-CTLA-4 showed a higher PFS rate compared to anti-PD-1 alone, with 36% of patients' progression-free at 5 years, compared to 29% for anti-PD-1 monotherapy. However, this higher rate comes with a

significantly higher risk of severe toxicities, with 59% of patients experiencing at least grade 3 toxicities with combination therapy versus 23–28% with monotherapy<sup>2</sup>. Despite these risks, some patients still require combination therapy to achieve optimal outcomes, underscoring the need to refine our ability to identify predictive biomarkers and better select those most likely to benefit from combination versus monotherapy.

Tumour mutation burden (TMB), the number of somatic mutations per megabase (mut/Mb) of the tumour genome, serves as a surrogate for the neoantigenic load of a tumour and, accordingly, has been linked to tumour

<sup>1</sup>Melanoma Institute Australia, The University of Sydney, Sydney, NSW, Australia. <sup>2</sup>Faculty of Medicine and Health, The University of Sydney, Sydney, NSW, Australia. <sup>3</sup>Charles Perkins Centre, The University of Sydney, Sydney, NSW, Australia. <sup>4</sup>Royal Prince Alfred Hospital and NSW Health Pathology, Sydney, NSW, Australia. <sup>5</sup>Department of Internal Medicine and Medical Specialties (DiMI), University of Genoa, Genoa, Italy. <sup>6</sup>Westmead and Blacktown Hospitals, Sydney, NSW, Australia. <sup>7</sup>The Canberra Hospital, Canberra, ACT, Australia. <sup>8</sup>College of Science and Medicine, Australian National University, Canberra, ACT, Australia. <sup>9</sup>Mater Hospital, North Sydney, Sydney, NSW, Australia. <sup>10</sup>Royal North Shore Hospital, Sydney, NSW, Australia. <sup>11</sup>Champalimaud Foundation, Lisbon, Portugal. <sup>12</sup>These authors contributed equally: Richard A. Scolyer, Georgina V. Long, Ismael A. Vergara, James S. Wilmott. ✉e-mail: [james.wilmott@sydney.edu.au](mailto:james.wilmott@sydney.edu.au)

immunogenicity and response to immunotherapies. The KEYNOTE-158 trial investigated single-agent pembrolizumab (anti-PD-1) in solid tumours, showing improved response rates for patients with high TMB ( $\geq 10$  mut/Mb)<sup>4</sup>. This finding prompted the United States Food and Drug Administration (FDA) to grant approval of pembrolizumab for metastatic solid tumours with high TMB as assessed by FoundationOne CDx® (F1CDx) testing. Clinical assessment of TMB often utilises formalin-fixed paraffin-embedded (FFPE) tissue, next-generation sequencing (NGS) targeted panels, and tumour-only variant calling due to practical constraints. Although targeted panels have been shown to have similar performance and low variability compared to whole exome sequencing for TMB estimation on high TMB tumours such as cutaneous melanoma<sup>5,6</sup>, commercial panels exhibit significant variation in target regions, included genes, variant callers, germline variant filtering methods, and even in the defining mutation types that contribute to TMB<sup>7,8</sup>. Given its clinical utility, the consistency of TMB estimation needs to be validated across the target panels.

Neoantigens predicted from somatic mutations via the binding affinity of mutated neopeptides to MHC molecules are another potential biomarker for ICI treatments<sup>9</sup>. An association with improved response and survival has been observed in melanoma patients treated with ICIs who exhibit higher neoantigen loads<sup>10–12</sup>. Despite the challenges in identifying recurrent tumour-specific neoantigens shared across patients<sup>10</sup>, neoantigen vaccines have demonstrated the ability to induce tumour infiltration and promote the long-term persistence of neoantigen-specific T cells<sup>13</sup>. Therefore, a deeper understanding of tumour-specific neoantigens is crucial, and the utility of neoantigen quantification via NGS panels remains to be seen.

To address these issues, we conducted targeted NGS based TMB testing utilising three targeted panels, including the QIAseq TMB IO (QIAGEN), Illumina TSO500 and F1CDx (Foundation Medicine), to assess real-world prospective reproducibility of TMB. We then investigated the association between individual somatic mutations ( $N = 198$ ), neoantigens ( $N = 135$ ), as well as TMB and neoantigenic load ( $N = 135$ ) with response to ICI therapies in patients with metastatic melanoma.

## Results

### Prospective TMB estimation is highly reproducible across NGS panels and laboratories

TMB estimation was conducted on 62 samples using the QIAGEN workflow, with default settings in a prospective manner within the Melanoma Institute Australia's translational research laboratory (in-house). To assess reproducibility of TMB estimation and driver mutation status (*BRAF*, *RAS*, *NF1*), 27/62 samples were also tested via the TSO500 panel within Lab1, 43/62 samples TSO500 within Lab2 and 30/62 samples using the F1CDx, an FDA-approved method. Numbers vary due to sample availability and the prospective nature of the testing. All samples used in the cross-laboratory comparison passed all quality controls (see Methods). TMB values derived from the QIAGEN workflow showed significantly positive correlations with the TSO500 derived TMB (*Spearman's rho*<sub>both</sub> = 0.83,  $p$ : Lab1 =  $4.4 \times 10^{-8}$  and Lab2 =  $5 \times 10^{-12}$ ). When classifying patients into TMB high and low groups (based on 10 mut/Mb), there was no significant difference between the QIAGEN workflow and any lab using TSO500 (*McNemar's test p*: Lab1 = 0.22, Lab2 = 1) (Fig. 1a, b). Only one sample was identified as having a high TMB (defined as  $\geq 10$  mut/Mb) via the QIAGEN workflow and a low TMB in Lab2 with TSO500 (TMB<sub>QIAGEN</sub> = 134.5 vs TMB<sub>Lab2</sub> = 0.8). This was due to overestimation of the low allele fraction (AF) (5–9%) variants in the Qiagen TMB estimation. The QIAGEN workflow positively correlated with F1CDx (*Spearman rho* = 0.94,  $p = 1.1 \times 10^{-14}$ ), and both displayed identical TMB two-class estimations (*McNemar's test p* = 1) (Fig. 1c and Table S1).

Patients identified to have *BRAF* and *RAS* mutations in their melanoma via the QIAGEN workflow had the same melanoma molecular subtype designated using the TSO500 panel with similar AFs across laboratories. However, 8 out of 22 QIAGEN workflow *NF1*-melanoma patients did not have any *NF1* mutation in their melanoma based on TSO500 in Lab1 or Lab2. Among these, 2/8 patients with high AFs (73.5%,

60.4%) but were found to lack of coverage of those particular *NF1* regions in the TSO500 panel (Fig. 1d). One sample with a *NF1* mutation at 12.2% AF was not reported in Lab1. For the rest of the inconsistent *NF1*-mutants, the differences were associated with the low AFs of the *NF1* mutations (range 2.6–7%), suggesting a potential impact of tumour purity on the concordance across panels. In the case of F1CDx panel testing, the same *BRAF*, *KRAS* and *NF1* mutations detected with QIAGEN were identified at similar AFs (Fig. 1e) with all captured driver mutations present at AFs greater than 10% (range: *BRAF* 16.6–75%, *KRAS* 88.1%, and *NF1* 19.7–91.6%) (Table S1). These results indicate an excellent overall reproducibility across panels for TMB and driver mutations, with potential missed mutations in *NF1* based on TSO500 due to lack of coverage in specific regions.

### Clinical characteristics of the cohort

A separate cohort of 198 patients with advanced melanoma who received anti-PD-1 (PD1) or combination anti-CTLA-4 plus anti-PD-1 (IPI + PD1) therapies, with samples that passed quality controls and had sufficient tumour content (five samples excluded due to AFs < 10% in *BRAF* or *RAS* driver mutations), were processed for TMB estimation and mutation profiling with the QIAGEN workflow. The median age in this cohort was 63.5 years. Response as classified based on 6 months progression-free survival status into responders (PFS  $\geq 6$  months), with a significantly older cohort than non-responders (PFS < 6 months) (median age responders = 67 years, non-responders = 61 years,  $p = 0.04$ ). Non-responders had a higher proportion of acral and mucosal melanomas compared to responders ( $p = 0.005$ ). The majority of patients had *BRAF/RAS/NF1* driver mutations in their melanoma with only 14.1% being triple wild type (TWT). There were no significant differences in sex or treatment type between responders and non-responders ( $p > 0.05$ ) (Table 1 and Table S2).

### TMB is associated with response to ICIs and *NF1* mutation status

Given the concordant results observed above for TMB estimation, QIAGEN workflow-derived TMB (non-synonymous mutations only) and driver mutation status were investigated for associations with response to ICI therapies. The TMB values ranged from 0 to 668 mut/Mb (median: 13 mut/Mb). Melanomas of cutaneous non-acral origin and from older and male patients showed significantly higher TMB values compared to melanomas from other tissue origins, younger and female patients (median TMB: 15.2 mut/Mb in cutaneous melanoma versus 6.5 mut/Mb in non-cutaneous melanoma, 18 mut/Mb in older patients ( $\geq 65$  as older patients) versus 11.3 mut/Mb in younger patients, and 15.4 mut/Mb in male patients versus 11.3 mut/Mb in female patients;  $p = 4.8 \times 10^{-4}$ , 0.04 and 0.03, respectively).

Responders had significantly higher TMB compared to non-responders (median: 20.6 mut/Mb vs 9.5 mut/Mb,  $p = 2.6 \times 10^{-5}$ ) (Fig. 2a). Patients with a high TMB ( $\geq 10$  mut/Mb) had significantly longer median PFS compared to patients with low TMB (38.6 mo vs 3.8 mo; log-rank  $p = 2.9 \times 10^{-4}$ ). Furthermore, the high TMB class had a significantly higher proportion of responders compared to the low TMB class (Fisher's exact test  $p = 0.001$ , Fig. 2b). These differences were observed regardless of treatment groups (IPI + PD1: 58.7 months, 64.2% in high TMB patients versus 4.6 months, 38.9% in low TMB patients, log-rank  $p = 0.003$  and Fisher's exact test  $p = 0.006$ ; PD1: 21.6 months, 59.6% in high TMB patients versus 3.5 months, 36% in low TMB patients, log-rank  $p = 0.03$  and Fisher's exact test  $p = 0.09$ ), with a weaker association in the PD1 group likely due to the smaller cohort size (Table 1 and Table S2).

Melanomas from patients with *NF1* mutations ( $n = 55$ ) had the highest median TMB value (42 mut/Mb), followed by *RAS* ( $n = 44$ , 12.5 mut/Mb), *BRAF* ( $n = 71$ , 9.4 mut/Mb), and TWT ( $n = 28$ , 2.7 mut/Mb) subtypes. *NF1*-mutant patients had significantly higher TMB values than *BRAF*- and *RAS*-mutant patients ( $p = 2.5 \times 10^{-10}$  and  $1.5 \times 10^{-6}$ ). *RAS*-mutant patients had significantly higher TMB values than *BRAF*-mutant patients ( $p = 0.04$ ) (Fig. 2c). While *NF1*-mutant patients had the longest median PFS (11.8 months) compared to other mutational subtypes (*BRAF*: 5.3 months, *RAS*: 11.4 months, TWT: 8.7 months), these differences were not statistically significant (Fig. 2d). The *NF1*-mutant group had the highest proportion of

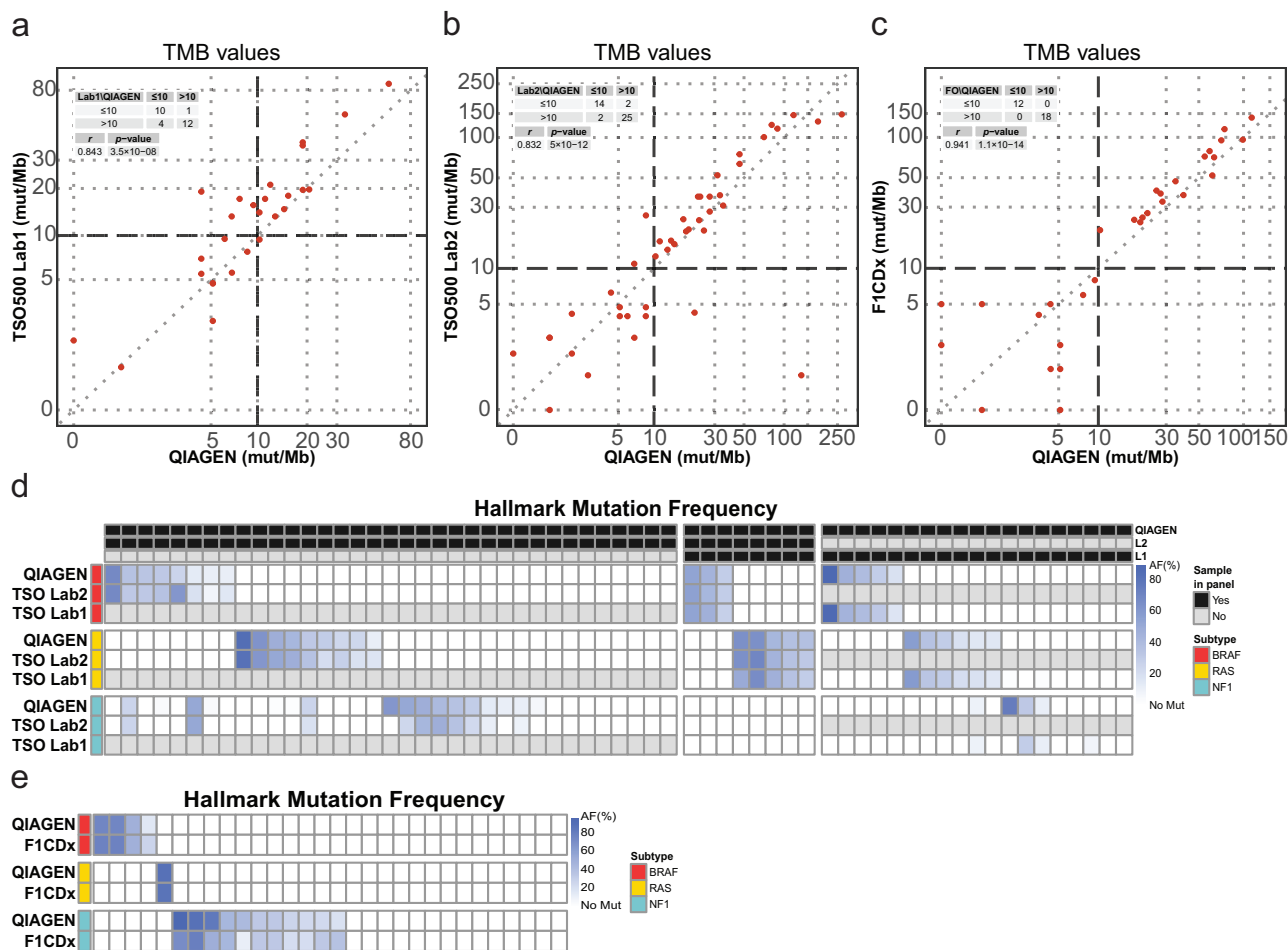


**Fig. 1 | TMB and melanoma driver mutations across NGS panels and laboratories.** TMB values between inhouse QIAGEN workflow and **a** TSO500 Lab1, **b** TSO500 Lab2, and **c** F1CDx. The correlations between TMB values are calculated by Spearman's rank correlation coefficient. TMB larger or equal than 10 mut/Mb is

used to define high TMB. Heatmap of AFs in melanoma driver mutations between QIAGEN and **d** TSO500, and **e** F1CDx, with row for each driver mutation and column for each sample. Samples not processed in Lab1 or Lab2 are indicated in grey.

responders (59.1%), while the *BRAF*-mutant group had the lowest proportion (46.5%), with these differences not reaching statistical significance in either the entire cohort or when separated by treatment (PD1-alone or IPI + PD1) (Tables 1 and S2).

No significant difference in TMB values was observed between major mutation subclasses within each driver gene (*BRAF* V600E versus V600K, *RAS* Q61 versus G12/13, and *NF1* missense versus nonsense mutations) (Fig. 2e). Patients with class-I *BRAF* mutations had overall lower TMB values than patients with other classes of *BRAF* mutations ( $p = 0.07$  against class-II, 0.02 against class-III, and  $6 \times 10^{-4}$  against no class) (Fig. 2f).

**Higher proportion of UV damage signatures is associated with ICI response**

In agreement with prior studies<sup>14</sup>, most single nucleotide variants were C > T, with melanomas of acral and mucosal origin displaying a lower prevalence of C > T and higher T > C/G changes. C > T transitions were similar among response status, age, and sex (Figs. 3a and S3). Pooled assessment of mutational signatures across melanomas showed prevalent UV damage (UV signatures SBS7a-d = 53.5% across patients), meanwhile melanomas from responders had a borderline significantly higher proportion of UV damage signatures compared to melanomas from non-responders (60.6% versus 45.7%,  $p = 0.05$ ) (Fig. 3b). Melanomas of cutaneous non-acral origin showed a higher proportion of UV damage signatures compared to melanomas of other origins (59.2% to 12.5%,  $p = 1.4 \times 10^{-5}$ ). Male and older patients also displayed significantly higher

proportions of UV damage signatures (59% versus 43.7% for females,  $p = 0.04$ ; 60.8% versus 46.5% for younger patients,  $p = 0.05$ ) (Fig. S4).

**PTPRD mutation is associated with better response and longer PFS**

We next extended our assessment of recurrently mutated genes and their association with PFS and response, focusing on likely-clonal mutations (AF > 10%). *BRAF* ( $N = 90$ , 46.6%), *LRP1B* ( $N = 79$ , 40.9%), *NRAS* ( $N = 50$ , 25.9%), *ROS1* ( $N = 49$ , 25.4%), and *GRIN2A* ( $N = 43$ , 22.3%) were identified as the top 5 recurrently mutated genes in this cohort (Fig. 4a, b and Table S3). *BRAF* and *RAS* melanoma hallmark mutations were mutually exclusive, except for one non-responder (*BRAF* V600E = 63.8% and *NRAS* G61K = 28.5%) and one responder (*BRAF* V600E = 25% and *KRAS* G61H = 24%).

Univariate logistic regression models weighted for confounding variables (TMB, age, sex, and cutaneous vs non-cutaneous), revealed that patients with melanomas harbouring *PTPRD* mutations ( $N = 35$ , 18.1%) showed a significantly better response and longer PFS than melanomas that were *PTPRD* wildtype, in both the entire cohort ( $OR_{weighted} = 1.89$  adj- $p = 0.01$ ;  $HR_{multi} = 0.49$   $p = 0.03$ ) and the IPI + PD1-treated group ( $OR_{weighted} = 1.9$  adj- $p = 0.05$ ) (Figs. 4c-e and S5). Patients with *FLT4*-mutant melanomas ( $N = 24$ , 12.4%) demonstrated longer PFS in both the entire cohort ( $HR_{multi} = 0.37$   $p = 0.02$ ) and in the PD1-treated group ( $HR_{multi} = 0.18$   $p = 0.02$ ) (Fig. 4d, g). Mutational status in *GRIN2A* ( $N = 43$ , 22.3%) and *DMD* ( $N = 33$ , 17.1%) showed association with better response

**Table 1 | Clinical characteristics of patients**

Characteristic		All (N = 198)	Responder (N = 104)	Non-responder (N = 94)	p-value
Age, median (IQR) years		63.5 (19-93)	67 (19-93)	61 (27-88)	0.0405 <sup>a</sup>
Sex, No. (%)	Female	71 (35.9)	32 (30.8)	39 (41.5)	0.1383 <sup>b</sup>
	Male	127 (64.1)	72 (69.2)	55 (58.5)	
Treatment, No. (%)	IPI + PD1	121 (61.1)	64 (61.5)	57 (60.6)	1 <sup>b</sup>
	PD1	77 (38.9)	40 (38.5)	37 (39.4)	
Cutaneous melanoma, No. (%)	Yes	174 (87.9)	98 (94.2)	76 (80.9)	0.0045 <sup>b</sup>
	No	24 (12.1)	6 (5.8)	18 (19.1)	
Melanoma subtypes, No. (%)	<i>BRAF</i>	71 (35.9)	33 (31.7)	38 (40.4)	0.5313 <sup>b</sup>
	<i>RAS</i>	55 (27.8)	31 (29.8)	24 (25.5)	
	<i>NF1</i>	44 (22.2)	26 (25)	18 (19.1)	
	TWT	28 (14.1)	14 (13.5)	14 (14.9)	
Median PFS (months)	IPI + PD1	6.8	24.8	2.3	
	PD1	7.8	30.2	0	
>12 months PFS, No. (%)	IPI + PD1	50 (25.3)	50 (25.3)	0 (0)	
	PD1	30 (7.6)	30 (7.6)	0 (0)	

Responder defined as PFS ≥ 6 months.

<sup>a</sup>Mann–Whitney test.

<sup>b</sup>Fisher’s Exact Test.

(*GRIN2A*:  $OR_{weighted} = 2.07$   $adj-p < 0.01$ ; *DMD*:  $OR_{weighted} = 1.8$   $adj-p = 0.02$ ) in the entire cohort of both PD1 alone and IPI + PD1 (Fig. 4c). Patients in the IPI + PD1-treated group showed favourable responses when their melanomas contained *TP53*-mutations ( $N_{IPI+PD1} = 18$ , 15.4%) or *MYOCD*-mutations ( $N_{IPI+PD1} = 15$ , 12.8%) (*TP53*:  $OR_{weighted} = 2.09$   $adj-p = 0.03$ ; *MYOCD*:  $OR_{weighted} = 4.02$   $adj-p < 0.001$ ) (Fig. 4e), as well as longer PFS with *KMT2D*-mutations ( $N_{IPI+PD1} = 15$ , 12.8%,  $HR_{multi} = 0.27$   $p = 0.02$ ) (Fig. 4f). Significantly worse outcomes were observed in patients with *HERC1*-mutant ( $N = 23$ , 11.9%) and *ALPK2*-mutant ( $N = 29$ , 15%) melanomas (*HERC1*:  $OR_{weighted} = 0.52$   $adj-p < 0.01$ ; *ALPK2*:  $OR_{weighted} = 0.61$   $adj-p = 0.04$ ).

One mutation in the catalytic subunit of *PIK3CA* (I391M,  $N = 27$ , 14%), which passed all somatic filters and has been reported as both a germline and somatic variant (COSM328028, population frequency of 6.6%, Figure S6), has been highlighted by prior studies to be a frequent alteration in patients with multiple primary melanomas [15]. The *PIK3CA* I391M variant was associated with better response and longer PFS in the entire cohort ( $OR_{weighted} = 2.19$   $adj-p < 0.01$ ;  $HR_{multi} = 0.44$   $p = 0.03$ ) (Table S4–5).

**Neoantigen loads have enhanced predictive value for response and PFS compared to TMB**

The utilisation of TMB as a proxy for neoantigen load, as well as the growing interest in neoantigen-based therapies, prompted us to evaluate the added value of measuring neoantigen load directly from the QIAGEN workflow mutational profiles. To achieve this, we determined the HLA class I and II types for somatic variants called from 135 patient samples, combined with clinical HLA typing of matched blood to measured the binding affinity of the resulting neopeptides to their HLA class I and II alleles for each non-synonymous mutation in each melanoma (see “Methods”). While neoantigen loads were found to be significantly and positively correlated to TMB values (Spearman  $\rho = 0.86$ ,  $p < 0.001$ ), large variability in the neoantigen load was observed within ranges of TMB (Fig. 5a).

As observed with TMB (Fig. 2a), responders showed significantly higher neoantigen load values compared to non-responders (median 10.5 versus 6 neoantigens, respectively,  $p = 0.01$ ) (Fig. 5b). Still, assessment of total neoantigen load as well as distinct subsets of neoantigens showed enhanced predictive value for patients treated with ICI compared to TMB. In the population of patients treated with PD1 alone, total neoantigen load

was significantly associated with response, a result not achieved with TMB as a numerical value ( $OR = 1.006$   $p = 0.07$  for neoantigen load versus  $OR = 1.006$   $p = 0.42$  for TMB) (Fig. 5c). Furthermore, the strength of the association for the IPI + PD1 patient group was stronger for neoantigen load ( $OR = 1.209$   $p = 0.02$ ) compared to TMB ( $OR = 1.025$   $p = 0.08$ ).

We then focused on the assessment of neoantigen load per HLA class II type. This showed that the subset of strong binders (see Methods) to HLA class II alleles resulted in an increase in prediction power for response and PFS compared to TMB values (as measured by better OR and HR values, and  $p$ -values of stronger significance) in the entire cohort as well as within PD1 and IPI + PD1 treatment groups (Fig. 5c, d and Table S6). These results suggest that the total neoantigen load, as well as subsets of neoantigens carry enhanced predictive value in the context of response to ICI treatment in melanoma patients.

**Recurrently mutation hotspots encode neoantigens associated with improved ICI outcome**

To investigate the association between individual predicted neoantigens and ICI outcomes in patients, we first assessed the neoantigenicity and predictive value from recurrently mutated genes across the cohort. We found that *RAC1* P29S ( $N = 13$ , 9.6%), *NRAS* Q61\* ( $N = 13$ , 9.6%), and *BRAF* V600\* ( $N = 18$ , 13.3%) more commonly bind to multiple HLA-A alleles (Fig. S7a). Several trends of association were identified, albeit not reaching statistical significance. Patients with *BRAF* V600\*:HLA-A binding pairs showed lower proportion of responders (44.4% versus 53.0% for non-*BRAF* V600\*:HLA-A paired patients,  $p = 0.61$ ) and shorter median PFS (2.8 versus 9.8 months for non-*BRAF* V600\*:HLA-A paired patients,  $p = 0.61$ ) than others (Fig. S7b, S8a). However, patients with *RAC1* P29S:HLA-A and *NRAS* Q61\*:HLA-A pairs had trends of higher proportion of responders and longer PFS (*RAC1* P29S:HLA-A: 69.2% versus 50% for non-*RAC1* P29S:HLA-A paired patients  $p = 0.25$ , and median PFS 21.6 versus 5.5 months  $p = 0.71$ ; *NRAS* Q61\*:HLA-A: 61.5% versus 50.8% for non-*NRAS* Q61\*:HLA-A paired patients  $p = 0.57$ , median PFS 38.6 versus 7.4 months,  $p = 0.33$ ) (Fig. S7b, S8b and c). In the case of *PTPRD*, associated with favourable ICI outcomes described above, no differences in response or PFS were identified between neoantigenic mutants and non-binding mutants (Fig. S9), indicative of its predictive value independent of the neoantigenicity of the individual mutations in that gene.

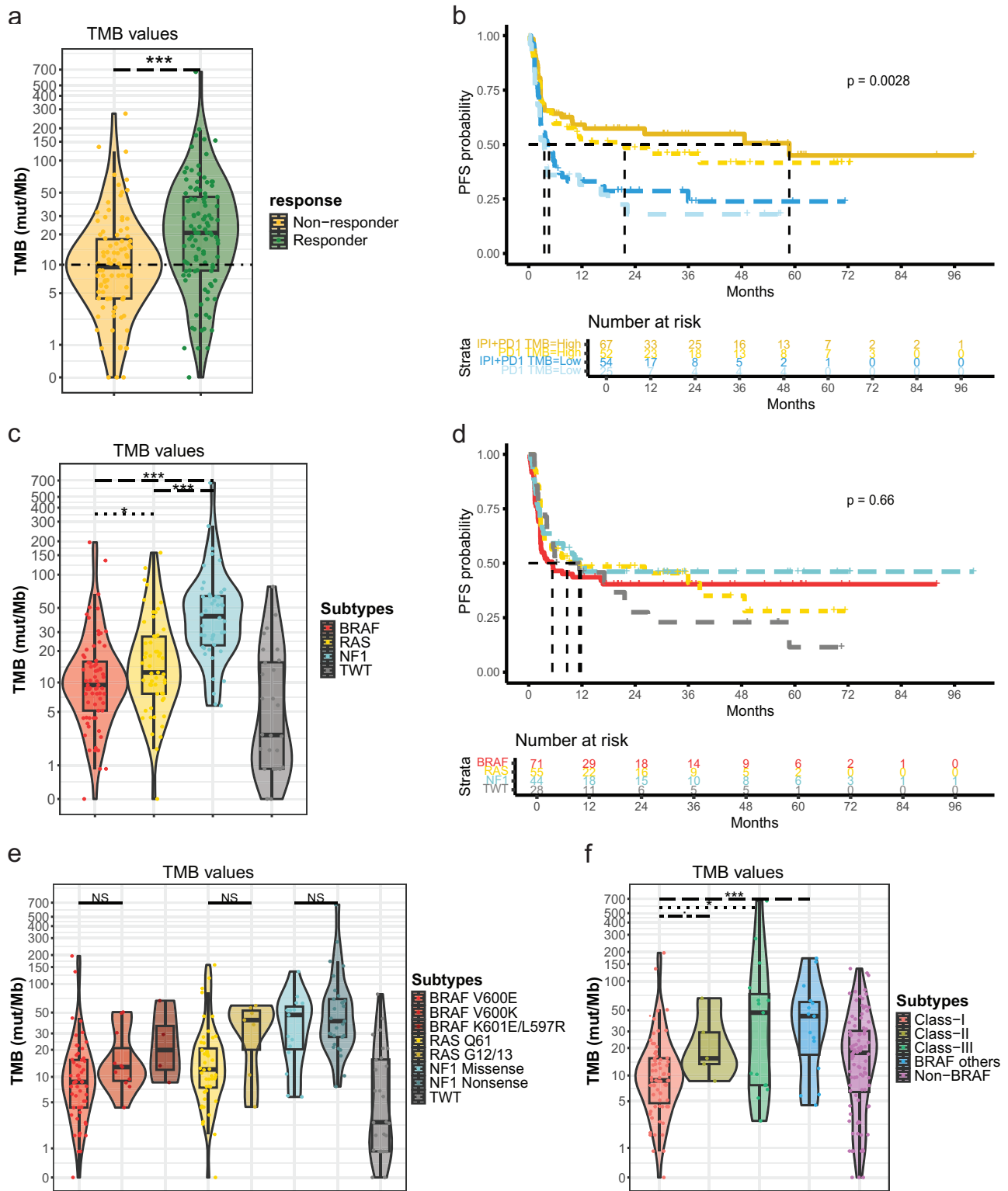


**Fig. 2 | TMB values and mutational subtypes against PFS and response to treatment.** **a** TMB values between responders and non-responders. **b** Kaplan–Meier curves of TMB classes in different treatments. **c, d** TMB values and Kaplan–Meier

curves among mutational subtypes. **e, f** TMB values among detailed mutation subtypes, and different *BRAF* classes. *p* value smaller than 0.1 (·), 0.05 (\*), 0.001 (\*\*\*) and no significance (NS).

More generally, beyond hotspots, several mutations in recurrently mutated genes encoded neoantigens associated with improved PFS, including *NF1*, *ROS1*, *GRIN2A*, *MYOCD* and *ERBB4*, compared to patients with a non-neoantigenic mutation (non-binding), as well as wild type patients.

Patients with melanomas harbouring neoantigenic *NF1* mutations had a significantly higher proportion of responders than mutated non-binding patients and patients without somatic clonal *NF1* mutations (83.3% for neoantigenic *NF1*-mutants versus 30% for mutated non-binding mutants *p* = 0.03, and 50.4% for other patients, *p* = 0.04). There was a trend towards a

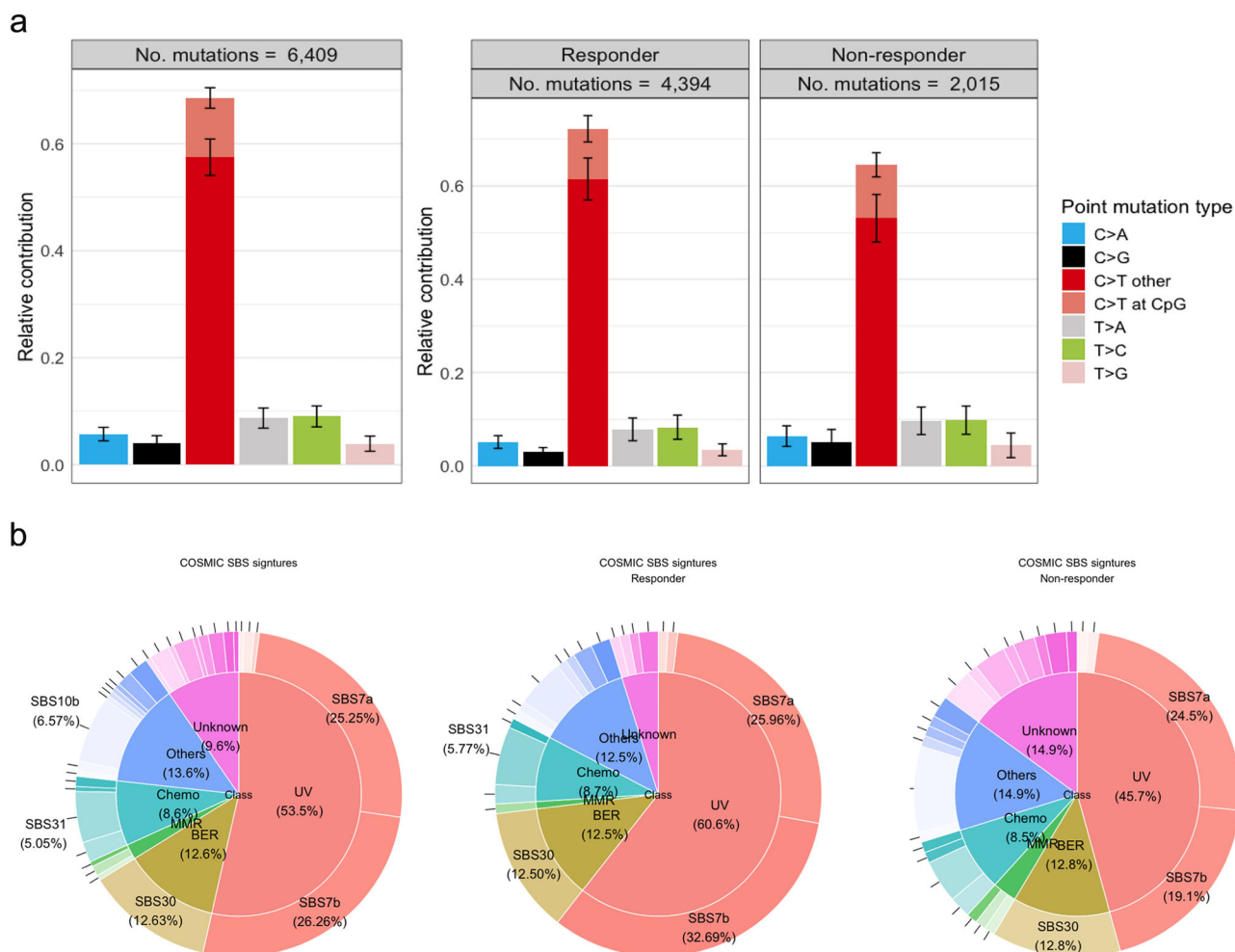


**Fig. 3 | Patients mutation profile and signature.** **a** SNV distribution in this cohort and across response status, where error bars indicate 95% confidence interval across samples. **b** Proportions of the most contributed SBS signature among patients. UV: Ultraviolet light exposure related SBS signatures. MMR: DNA mismatch repair

related signatures. BER: DNA base excision repair related SBS signatures. Chemo: chemotherapy treatment related SBS signatures. Unknown: unknown SBS signatures. Others: other kinds of SBS signatures.

longer PFS in patients with neoantigenic *NF1* mutations compared to non-binding patients (median PFS = 48.7 months vs 3 months log-rank  $p$ -value = 0.07). However, there was no significant difference in PFS when compared to patients without somatic clonal *NF1* mutations (median PFS = 7.4 months, log-rank  $p$ -value = 0.3) (Fig. 6a, c).

Patients carrying neoantigenic mutations in the *ROS1* gene had a trend towards longer PFS compared to non-binding patients and patients without somatic *ROS1* mutations (median PFS was not achieved for neoantigenic *ROS1* mutants versus 3.2 months, log-rank  $p$ -value = 0.09, and 5.5 months for patients without somatic *ROS1*-mutant, log-rank  $p$ -value = 0.07), with no significant difference in response (Fig. 6b, c). Importantly, while mutations in either *NF1* or *ROS1* genes were significantly associated with higher TMB, no significant difference in TMB was found between mutated binding and non-binding patients (Fig. 6d, e). Inspection of binding and non-binding mutations in these genes revealed those with predicted binding affinity to MHC classes were all missense mutations, while the mutations in non-binding patients in *NF1* and 6 out of 9 patients in *ROS1* were nonsense mutations. These results suggest that different mutation types in recurrently mutated genes may have a distinct impact on tumour aggressiveness versus elicitation of an immune response, adding biological complexity that can lead to clinical differences after ICI treatment.

## Discussion

This study confirms the reproducibility and clinical utility of TMB estimation. Furthermore, we identified additional value in neoantigen profiling, in particular subsetting *NF1* driven tumours by neoantigenicity for association with response to immunotherapies using a commercial NGS testing panel and variant calling pipelines.

Our findings support a high concordance in TMB estimation when assessed as a continuous variable and as a categorical variable (based on a threshold of 10 mut/Mb)—across both laboratories and sequencing panels. Furthermore, we observed a strong concordance in the presence and AFs of *BRAF* and *RAS* driver mutations between these panels and across laboratories. Although all laboratories reported similar AFs when capturing the same *NF1* mutations, some *NF1* mutations detected by the QIAGEN panel were not identified by the TSO500 panel. The majority of these discordant *NF1* mutations predominantly exhibited low AFs, while in two patients, high AF *NF1* mutations were missed as the genomic regions were not targeted by the TSO500 panel, likely due to the long genomic span of this gene (~350 kb long gene with 60 exons)<sup>16</sup>. Review of the low AF mutations (between 2.5 and 9%) that passed QIAGEN variant calling QC suggested that the higher read depth of the QIAGEN workflow compared to TSO500 allowed for the identification of potential subclone variants.

The spectrum of mutational signatures agreed with the prevalence of UV damage observed in cutaneous versus non-cutaneous melanoma, even

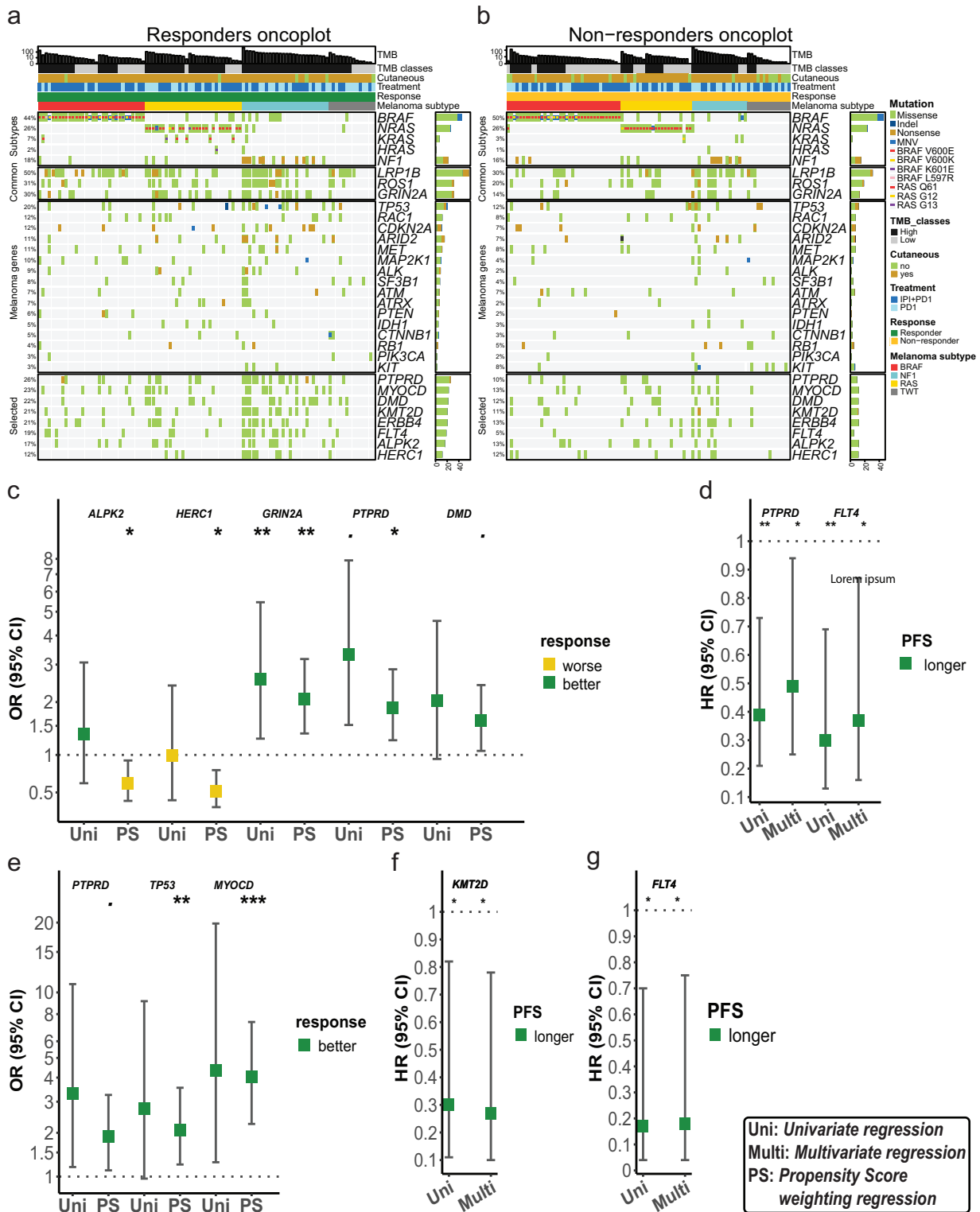


**Fig. 4 | Mutational profiles and associations between single genes, response and PFS.** a, b Oncoplots of major somatic mutations in responders and non-responders using genes associated with melanoma molecular subtype, commonly mutated, melanoma related genes and genes highlighted genes in this study. c, e Correlation of single gene mutation status with response was estimated by OR in univariate logistic regression with (labeled with PS) and without (labeled with Uni)

propensity scores in c entire cohort and e IPI + PD1 treated patients with relative adjusted-*p* values. Correlation of single gene mutation status to PFS was estimated by HR in univariate (labeled with Uni) and multivariate (labeled with Multi) CoxPH regressions in d entire cohort, f IPI + PD1 treated, and g PD-1 treated patients with relative *p* value smaller than 0.1 (-), 0.05 (\*), 0.01 (\*\*), and 0.001 (\*\*\*)

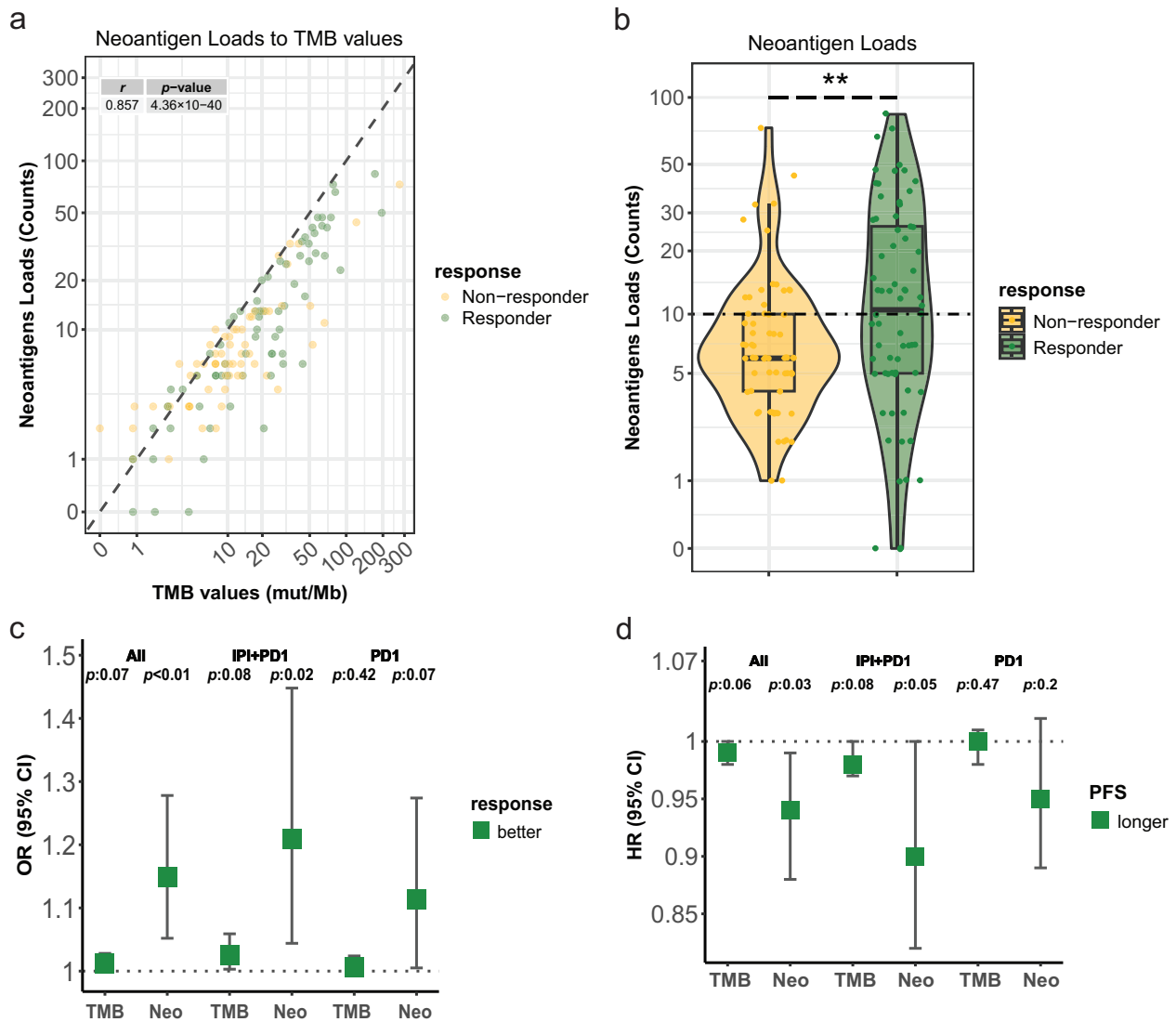


**Fig. 5 | Association of neoantigen load and TMB values with response and PFS.** **a** Scatterplot of neoantigen load versus TMB values colored by response group. **b** distribution of neoantigen load against response status. **c** OR of univariate logistic

regression for TMB and class-II strong-binding neoantigen load, and **d** HR in univariate CoxPH regression for TMB and class-II strong-binding neoantigen load in the entire cohort, as well as within treatment modality.

via NGS panel testing<sup>17</sup>. This study validates findings from other study showing that cutaneous melanoma exhibits a significantly high proportion of UV damage signatures and increased response rate to immunotherapies<sup>18</sup>. However, the prevalence of patients with UV-dominated mutation signatures was lower in our cohort; this may be due to the targeted panel design and tumour-only variant filtering processes (for example, only non-synonymous were selected) compared to whole genome-based studies<sup>14</sup>. Therefore, this study may underestimate the contribution of UV damage. Previous studies have reported more favourable outcomes from ICIs in males compared with females<sup>19,20</sup> and in older versus younger patients<sup>21</sup>. Also, an increased TMB has been reported in male patients with metastatic melanoma versus females<sup>22</sup>. As expected, our study also reported that older and male patients have higher response rates to ICI treatments and displayed stronger association with UV damage signatures.

Analysis of single gene mutation status identified that *PTPRD* mutations are associated with longer PFS to ICI, independent of TMB values and other clinical variables, which may affect melanoma mutation profiles. A prior study reported a similar prevalence of *PTPRD* gene mutations in melanoma<sup>23</sup>. *PTPRD* mutations have also been reported to enhance response and overall survival (OS) in multiple cancer types, including melanoma, in larger cohort studies<sup>24-26</sup>. In non-small cell lung cancer,

deleterious mutations in the *PTPRD* phosphatase domain were associated with benefit from ICI treatments and were also independent of TMB<sup>27</sup>. In our cohort, additional neoantigen analysis revealed that these benefits are not associated with the predicted binding to HLA alleles and therefore may have biological functions.

*PTPRD* is a tumour suppressor gene (TSG) within the protein tyrosine phosphatase gene family and has been reported to suppress *STAT3* function through dephosphorylation. Mutations in *PTPRD* led to increase *STAT3* phosphorylation in head and neck cancer<sup>28</sup>, while expression of *PTPRD* negatively correlated with phosphorylated *STAT3* and *PD-L1* expression in hepatocellular carcinoma<sup>29</sup>. Responders have higher *PD-L1* gene expression and peritumoural *PD-L1*+ cell proportions in metastatic melanoma patients treated with ICIs<sup>30</sup>. Additionally, *PTPRD* is located at chromosome 9p, a region frequently subjected to loss of heterozygosity in cutaneous, acral and mucosal melanoma<sup>17</sup>; 9% of cutaneous melanoma patients have been reported to have a *PTPRD* homozygous deletion<sup>15</sup>. This suggests a potential two-hit inactivation mechanism in *PTPRD*-mutant melanomas. However, due to a lack of matched normal samples, copy number alteration analysis was not conducted in this study. Therefore, the impact of *PTPRD* loss-of-function and its association with *PD-L1* expression in melanoma warrants further investigation.

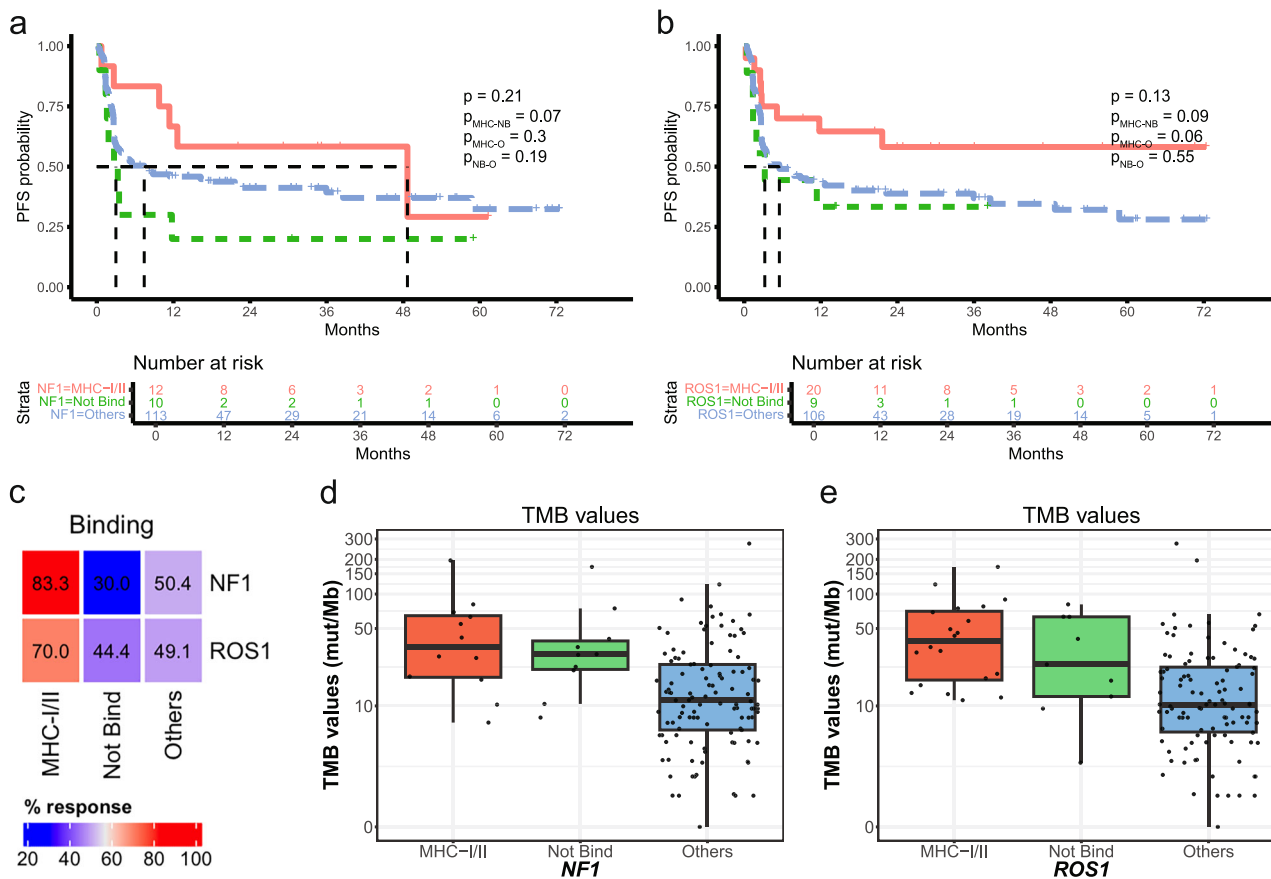


**Fig. 6 | Response and PFS for neoantigens from *NF1* and *ROS1*.** **a, b** Kaplan–Meier curves for PFS based on *NF1* and *ROS1* mutational and neoantigenic status. **c** Proportion of responders on *NF1* and *ROS1* mutations among neoantigenic binding status. MHC-I/II: neoantigens were predicted to bind MHC class-I or -II.

Not Bind: neoantigen was not predicted to bind any MHC class. Others: patients without mutations from this gene. **d, e** Boxplot of TMB values in *NF1* and *ROS1* across mutational and neoantigenic categories.

*PIK3CA* I391M is another candidate variant associated with improved response and PFS, independent of TMB and other clinical variables. Although the high population frequency and the distribution of AFs in this study identified this mutant as a potential germline variant, it has been reported as a common mutation in both primary and metastatic melanoma<sup>31,32</sup>. As an oncogene, *PIK3CA* active mutation can result in immune evasion and diminish the efficacy of anti-PD-1 treatment<sup>33</sup>. *PIK3CA* I391M has also been shown to promote cell proliferation<sup>34</sup>. However, the impacts of I391M on protein function and downstream pathways in the context of immunotherapies are still unclear. This study highlights a germline SNP with potential to predict benefit from ICIs.

In this study, we also sought to understand the additive prediction value of neoantigen load to that of TMB. First, we demonstrated the utility of TMB in stratifying response and PFS. TMB has been extensively reported to correlate with response and survival across multiple cancer types, including melanoma<sup>35,36</sup>. Beyond that, neoantigen load is positively associated with longer PFS in metastatic melanoma patients treated with anti-CTLA-4<sup>10</sup>, and in metastatic cancer patients treated with anti-PD-1<sup>12</sup>. Our study identified the enhanced value of neoantigen loads in predicting response and PFS regardless of MHC class. A recent study showed improved stratification of response in ICI-treated patients based on neoantigen burden compared to TMB<sup>37</sup>. Further, our study found that neoantigens which strongly bind to MHC class-II molecules provided the greatest increase in predictive power for response compared to TMB values in this study. MHC class-II presents a more diverse range of peptides to CD4<sup>+</sup> T-cells<sup>38</sup>. In a mouse model, tumour rejection required the expression of MHC class-II restricted neoantigens by tumour cells<sup>39</sup>. MHC class-II expressing cells were

spatially closer to Ki67<sup>+</sup>TCF1<sup>+</sup>CD8<sup>+</sup> T-cells, which are a predominant predictor of response in triple-negative breast cancer patients treated with ICIs<sup>40</sup>. These findings suggest a potentially predominant role for MHC class-II-mediated neoantigen presentation in modulating ICI response and survival.

The most frequent neoantigen-HLA binding pairs include several prevalent melanoma hotspot mutations. Our study shows that the predicted binding to HLA-A does not rescue the low proportion of responders and short PFS in *BRAF*-mutant melanoma patients. However, there are potential benefits that may arise from *NRAS* Q61\* and *RAC1* P29S neoantigens when bound to HLA-A. In a prior study, *NRAS* Q61K/R mutated neoantigens were reported to bind to HLA-A\*01:01 in 7% of melanoma patients, and the Q61 residue was shown to have potential binding capability to T cell receptors through the 3D structure of the peptide-HLA complex<sup>41</sup>. *RAC1* P29S can also be presented to T cells and activate T-cell-induced cytotoxicity against melanoma cells via binding to HLA-A\*02:01 in a mice model<sup>42</sup>. However, due to the small sample size after stratification, these analyses lack sufficient power to reach statistical significance. Additionally, higher TMB values in these patients may confound the true impact of these binding pairs.

This study identified two potential neoantigenic genes, *NF1* and *ROS1*. As a frequently mutated gene in cutaneous melanoma, *NF1* mutations have been associated with increased TMB and longer survival<sup>17,43</sup>. Our study showed trends towards improved response and PFS in *NF1*-mutated patients compared to those with wild-type *NF1*, though this did not reach statistical significance. Similarly, *ROS1* mutations, especially those in the protein tyrosine kinase region, have been illustrated as a favourable

biomarker for OS following ICI treatments in a pan-cancer cohort, as well as melanoma<sup>44–46</sup>. In our study, non-binding mutations in *NF1* and *ROS1* were mostly nonsense mutations. These patients had overall worse response and PFS compared to patients with binding mutations. In contrast, neoantigenic *NF1* and *ROS1* mutations were primarily missense mutations. These differences in response and PFS between binding status were not associated with TMB. Unlike missense mutations, nonsense mutations are predicted to generate fewer neoantigens due to nonsense-mediated RNA decay that degrade premature RNAs with nonsense mutations<sup>38</sup>. Therefore, although both missense and nonsense mutations may similarly impact gene expression, missense mutations are more likely to result in neoantigens with potential immunogenicity. However, while these findings were developed across multiple hospitals, all patients in the study were from an Australian cohort. Associations observed between mutation burden and specific driver events require further validation in geographically and demographically diverse populations to confirm the reproducibility and broader applicability of the findings.

We confirmed the real-world reproducibility of TMB estimation and melanoma subtype calling through targeted gene panels (QIAseq TMB, TSO500 and F1CDx) across laboratories. Although the targeted panel, by definition, does not include all exomes, limiting the ability to detect all genes and passenger mutations which may also contribute to the neoantigen load, this study reported improved response to ICIs in cutaneous melanoma, older and male patients with UV damage, as well as in patients with high TMB and neoantigen loads, as observed in previous studies. We further identified somatic mutations in the *PTPRD* gene and the germline SNP *PIK3CA* I391M as potential biomarkers associated with better response and longer PFS, independent of TMB values and clinical confounding variables. After integrating these findings with patient HLA typing, we highlighted that the binding affinity of neoantigens generated from *NF1* and *ROS1* to MHC class molecules is a key feature for long-term therapeutic benefit.

## Methods

### Patient cohorts and specimens

The prospective cohort included 198 patients who received immune checkpoint inhibitors anti-PD-1 or anti-PD1+anti-CTLA-4, with histologically confirmed stage III unresectable or IV melanoma as part of the Personalised Immunotherapy Platform (PIP-PREDICT, NCT06536257)<sup>47</sup>. All patients were enrolled in the study via written informed consent, and biospecimens were collected via the biospecimen bank of Melanoma Institute Australia. The study protocol was approved by the Sydney Local Health District Ethics Committee (2020/ETH00426). All procedures were carried out in accordance with the principles of the Declaration of Helsinki.

Patients with prior targeted therapy or adjuvant or neoadjuvant systemic immunotherapy were eligible. Pre-treatment, FFPE melanoma biopsies underwent pathological review, and those with a threshold of >20% tumour nuclei content were selected for targeted panel NGS testing. Patients were excluded due to lack of a suitable sample for NGS testing or insufficient nucleic acids available after extraction.

The patient's disease response was classified based on progression-free survival (PFS) into responders (defined as PFS ≥ 6 months) and non-responders (PFS < 6 months).

### DNA extraction

Macrodissection was performed prior to extraction to further enrich the sample for tumour regions. Genomic DNA extraction was performed using the AllPrep DNA/RNA FFPE Kit (cat. No. 80234, Qiagen) according to the manufacturer's instructions. Large tumours underwent separate DNA extractions on separate tissue using the High Pure FFPE DNA Isolation kit (cat. No. 06 650 767 001, Roche) when tissue size permitted.

### Targeted NGS panels and TMB estimation

**QIAseq human tumour mutational burden panel.** Somatic mutation burden was assessed using the QIAseq Targeted DNA Human Tumour Mutational Burden Panel (DHS-6600Z, QIAGEN) as per the

manufacturer's instructions. The entire workflow was performed at the Melanoma Institute Australia's translational research laboratory (in-house). Pre-test quality control of the DNA was performed using the QIAseq Library Quant Assay Kit (333314 QSTF-ILZ-N, QIAGEN). Samples failing the QIAseq Library Quant Assay had 250 ng of input DNA added as opposed to the standard 100 ng used for all samples that passed QC. Libraries were prepared as per the manufacturer's instructions and subsequently quantified using the Qubit dsDNA HS Assay (Q32851). Libraries were pooled, and quality controls were performed using TapeStation (Agilent). Paired-end 300 cycle sequencing was performed on the Illumina Novaseq (S4 flow cell, loading 175 pM without PhiX) or Nextseq 2000 (P2 flow cell, loading 175 pM without PhiX) instruments using QIAseq A Read 1 Primer as custom primer. FASTQ generation was performed on-board sequencer.

Variant detection and TMB estimation were performed using the predefined TMB workflow as part of the Biomedical Genomics Analysis plugin "Identify QIAseq DNA Somatic Variants with TMB Score" with default settings. Within the analysis workflow, samples were aligned to the reference genome (Homo.sapiens.GRCh38.v82), somatic single nucleotide variant called, germline variants filtered (Single Nucleotide Polymorphism database, dbSNP), and TMB (nonsynonymous somatic mut/Mb) estimated. Samples with low exon regions' coverage (<900,000 bp of panel targeted regions with >100X read depths) were excluded.

**TruSight oncology 500 panel (Illumina).** Samples were fragmented with a M-220 Focused-ultrasonicator (Covaris) using 80 ng of gDNA. To evaluate the peak size of the generated fragments, the samples were run on the 2100 Bioanalyzer Instrument (Agilent) using the High Sensitivity DNA Kit (Agilent). Libraries were prepared following the manufacturer's instructions and were quantified with the Qubit dsDNA HS Assay Kit (Thermo Fisher Scientific). A library concentration of at least 3–5 ng/μl was required to achieve efficient bead-based library normalisation. Normalised libraries were pooled together (maximum of eight libraries per pool incubated at 96 °C for 2 min). Two different dilutions were performed to obtain a final concentration of 1.5 pM. Sequencing was performed on NextSeq 500 platform using High Output reagents, 8 samples per flowcell and 300 cycles of sequencing in paired-end (Illumina). Furthermore, PhiX control at 1% (Illumina) was used as a sequencing control. Variant calling and estimation of TMB (nonsynonymous somatic mut/Mb) were done using DRAGEN TruSight Oncology 500 (TSO500) Analysis Software.

**FoundationOne.** The CDx assays were performed at Foundation Medicine. Data analysis and TMB reporting were performed by the College of American Pathologists (CAP)-accredited laboratory. This testing was performed as part of the MatchMEL trial (NCT02645149), with FoundationOne CDx tests performed and funded by Roche Products Pty Limited.

### Reproducibility of TMB

To assess reproducibility of TMB estimation and driver mutation status, TMB estimation was conducted on 62 samples using the QIAGEN workflow in a prospective manner. Then the same DNA was sent to two separate laboratories (laboratory 1 (Lab1), 43/62 samples, and laboratory 2 (Lab2), 27/62 samples) to generate TMB values using TSO500 workflow at each site. Additional validation of reproducibility was conducted using F1CDx on the same tumour biopsy for additional 30 samples.

### Melanoma driver mutation subtyping

Assessment of the melanoma mutation subtype was performed to classify samples into *BRAF* (codons 597, 600, and 601), *RAS* (*N/K/H/RAS* in codons 12, 13, and 61), *NF1* (damaging non-synonymous mutation) and triple wild type (TWT, lacking the prior mutations). All cases had prior routine clinical molecular diagnostic testing, which was checked for concordance with the mutation subtypes for *BRAF*, *NRAS*, *KRAS*, *HRAS* and *KIT*. Samples with

concordant mutation status were included in further analysis. Cases with a *BRAF* mutation were also classified into class-I/II/III based on Owsley et al.'s study<sup>48</sup>. Samples with AFs below 10% in *BRAF* and *RAS* driver mutations were regarded as low tumour purity and excluded from downstream analysis (Fig. S1a, S2).

### Somatic variants refinement

The QIAGEN TMB workflow filtered some known melanoma hotspots to improve the reproducibility of TMB estimation across cancers, for example, *BRAF* V600E filtered out as it appears in the dbSNP database (Fig. S1a). Therefore, for assessment of specific mutations outside of TMB estimation, further somatic variant identification was performed on the prefiltered variants passing QIaseq quality control (QC) to include all possible somatic variants. For assessment of inactivating mutations in TSGs, somatic variants predicted to be tolerated with SIFT score (score>0.05) were excluded<sup>49</sup>. The variants that passed QC steps were further annotated based on COSMIC, dbSNP and gnomAD<sup>50–52</sup>. Variants annotated within an inhouse curated set of recurrently mutated melanoma somatic mutation hotspot list were kept. Other variants in dbSNP or those in gnomAD with a population frequency  $\geq 0.1\%$  were excluded as germline variants. In the remaining variants, COSMIC labelled variants were selected if they were reported in >5 melanoma cases and had been confirmed as a somatic mutation, or if the reported gene had somatic mutations in >10 melanoma cases. For the remaining variants, TSGs were selected with SIFT score  $\leq 0.05$  and at least one reported case in melanoma within COSMIC. Finally, the potential homozygous threshold was set as >90% AF, unless any of the curated in-house hotspot (i.e. *BRAF* V600E) higher than 90% AF. Cancer Genome Interpreter (CGI)<sup>53</sup> was used to annotate known driver and passenger mutations (Fig. S1a).

### Mutation profile and signatures

After identification of somatic variants, single base substitutions (SBS) signatures list from COSMIC<sup>54</sup> was used to profile patients' mutational signatures on VCF files through MutationalPatterns v3.14.0 package<sup>55</sup>.

### Single gene mutation association with response and progression-free survival

To assess associations between gene mutation status and immunotherapy responses, a univariable logistic regression model was performed after matching the cohort based on mutation status. The matching process used propensity score (PS), which accounted for TMB, age, sex and tissue of origin (cutaneous melanoma versus other (acral and mucosal)) (Fig. S1b). Mutations in genes with AFs  $\geq 10\%$  were kept as a proxy to clonal mutations more likely to elicit a neoantigenic response. The propensity score (PS) weighting was performed to reduce the impact due to imbalance of confounding variables on mutation status, and the Standardised Mean Difference (SMD) was used to assess the balance<sup>56</sup>. SMDs < 20%<sup>57</sup> for all confounding variables were considered as balance in this study. R package *weightit* v1.1.0<sup>58</sup> was used to measure PS weights with average treatment effect method.

A multivariable Cox proportional hazard (CoxPH) model was performed to evaluate the impact of gene mutation status on PFS, adjusting for TMB class ( $\geq 10$  as high TMB), age ( $\geq 65$  as older patients), sex, and tissue of origin.

### HLA typing and neoantigen association with Immunotherapy responses

Clinical HLA typing of class-I HLA alleles A, B, and C, as well as class-II HLA DPB1, DQA1, DQB1, DRB3, DRB4, and DRB5 was performed on DNA extracted from the patients snap frozen whole blood sample using the HLA typing NGS panel (Illumina) at the Institute for Immunology and Infectious Diseases, Murdoch, Western Australia.

Previous somatic variants' VCF files were pre-annotated with VEP v102 using wildtype and frameshift plugins, as required by pVACtools v2.0.5. The pvacseq function of pVACtools was applied to identify

neoantigens from these VCF files and matched patients' HLA typing<sup>59</sup>, where MHCflurry and NetMHCpan were selected to estimate neoepitope binding affinity to MHC class-I, and NAlign and NetMHCIIpan were used to MHC class-II. The filtered default output was used for downstream analysis. The strong and weak binding thresholds percentiles used were <0.5% and <2% in MHC class-I, and <2% and <10% in MHC class-II, respectively<sup>60</sup>.

### Statistical analysis

Mann–Whitney test was applied between groups of numeric values. Fisher's Exact Test was applied between categorical variables and binary outcomes.  $p$ -value  $\leq 0.1$  and 95% confidence interval not cross 1 were used to select significant Odds Ratio (OR) and Hazard Ratio (HR). Benjamini–Hochberg (BH) method was applied to adjust  $p$ -values for multiple testing.

### Data availability

The datasets generated and analysed during the current study are part of an ongoing prospective study and are not publicly available due to the proprietary ownership of the data and the privacy of the patient cohort but are available from the corresponding authors on reasonable request.

### Code availability

The underlying code for this study is not publicly available but may be made available to qualified researchers on reasonable request from the corresponding author.

Received: 21 July 2025; Accepted: 27 November 2025;

Published online: 22 January 2026

### References

1. Ascierto, P. A. et al. Survival outcomes in patients with previously untreated BRAF wild-type advanced melanoma treated with nivolumab therapy: three-year follow-up of a randomized phase 3 trial. *JAMA Oncol.* **5**, 187–194 (2019).
2. Larkin, J. et al. Five-year survival with combined nivolumab and ipilimumab in advanced melanoma. *N. Engl. J. Med.* **381**, 1535–1546 (2019).
3. Schachter, J. et al. Pembrolizumab versus ipilimumab for advanced melanoma: final overall survival results of a multicentre, randomised, open-label phase 3 study (KEYNOTE-006). *Lancet* **390**, 1853–1862 (2017).
4. Marabelle, A. et al. Association of tumour mutational burden with outcomes in patients with advanced solid tumours treated with pembrolizumab: prospective biomarker analysis of the multicohort, open-label, phase 2 KEYNOTE-158 study. *Lancet Oncol.* **21**, 1353–1365 (2020).
5. Budczies, J. et al. Optimizing panel-based tumor mutational burden (TMB) measurement. *Ann. Oncol.* **30**, 1496–1506 (2019).
6. Merino, D. M. et al. Establishing guidelines to harmonize tumor mutational burden (TMB): in silico assessment of variation in TMB quantification across diagnostic platforms: phase I of the Friends of Cancer Research TMB Harmonization Project. *J. Immunother Cancer* **8**, <https://doi.org/10.1136/jitc-2019-000147> (2020).
7. Stenzinger, A. et al. Harmonization and standardization of panel-based tumor mutational burden measurement: real-world results and recommendations of the quality in pathology study. *J. Thorac. Oncol.* **15**, 1177–1189 (2020).
8. Vega, D. M. et al. Aligning tumor mutational burden (TMB) quantification across diagnostic platforms: phase II of the Friends of Cancer Research TMB Harmonization Project. *Ann. Oncol.* **32**, 1626–1636 (2021).
9. Gibney, G. T., Weiner, L. M. & Atkins, M. B. Predictive biomarkers for checkpoint inhibitor-based immunotherapy. *Lancet Oncol.* **17**, e542–e551 (2016).

10. Van Allen, E. M. et al. Genomic correlates of response to CTLA-4 blockade in metastatic melanoma. *Science* **350**, 207–211 (2015).
11. Hugo, W. et al. Genomic and transcriptomic features of response to anti-PD-1 therapy in metastatic melanoma. *Cell* **165**, 35–44 (2016).
12. Le, D. T. et al. PD-1 blockade in tumors with mismatch-repair deficiency. *N. Engl. J. Med.* **372**, 2509–2520 (2015).
13. Hu, Z. et al. Personal neoantigen vaccines induce persistent memory T cell responses and epitope spreading in patients with melanoma. *Nat. Med.* **27**, 515–525 (2021).
14. Hayward, N. K. et al. Whole-genome landscapes of major melanoma subtypes. *Nature* **545**, 175–180 (2017).
15. Stark, M. & Hayward, N. Genome-wide loss of heterozygosity and copy number analysis in melanoma using high-density single-nucleotide polymorphism arrays. *Cancer Res.* **67**, 2632–2642 (2007).
16. Bergoug, M. et al. Neurofibromin structure, functions and regulation. *Cells* **9**, <https://doi.org/10.3390/cells9112365> (2020).
17. Newell, F. et al. Comparative genomics provides etiologic and biological insight into melanoma subtypes. *Cancer Discov.* **12**, 2856–2879 (2022).
18. Andrews, M. C. et al. Predictive impact of tumor mutational burden on real-world outcomes of first-line immune checkpoint inhibition in metastatic melanoma. *JCO Precis Oncol.* **8**, e2300640 (2024).
19. Conforti, F. et al. Cancer immunotherapy efficacy and patients' sex: a systematic review and meta-analysis. *Lancet Oncol.* **19**, 737–746 (2018).
20. Jang, S. R. et al. Association between sex and immune checkpoint inhibitor outcomes for patients with melanoma. *JAMA Netw. Open* **4**, e2136823 (2021).
21. Kugel, C. H. et al. Age correlates with response to anti-PD1, reflecting age-related differences in intratumoral effector and regulatory T-cell populations. *Clin. Cancer Res.* **24**, 5347–5356 (2018).
22. Gupta, S., Artomov, M., Goggins, W., Daly, M. & Tsao, H. Gender disparity and mutation burden in metastatic melanoma. *J. Natl. Cancer Inst.* **107**, <https://doi.org/10.1093/jnci/djv221> (2015).
23. Zhang, W. et al. Association of PTPRT mutations with immune checkpoint inhibitors response and outcome in melanoma and non-small cell lung cancer. *Cancer Med.* **11**, 676–691 (2022).
24. Ou, C., Peng, Q. & Zeng, C. An integrative prognostic and immune analysis of PTPRD in cancer. *Math. Biosci. Eng.* **19**, 5361–5379 (2022).
25. Principe, D. R. Patients deriving long-term benefit from immune checkpoint inhibitors demonstrate conserved patterns of site-specific mutations. *Sci. Rep.* **12**, 11490 (2022).
26. Shang, X. et al. PTPRD/PTPRT mutation as a predictive biomarker of immune checkpoint inhibitors across multiple cancer types. *Front. Immunol.* **13**, 991091 (2022).
27. Sun, Y. et al. Identification and validation of tissue or ctDNA PTPRD phosphatase domain deleterious mutations as prognostic and predictive biomarkers for immune checkpoint inhibitors in non-squamous NSCLC. *BMC Med.* **19**, 239 (2021).
28. Peyser, N. D. et al. Loss-of-function PTPRD mutations lead to increased stat3 activation and sensitivity to STAT3 inhibition in head and neck cancer. *PLoS ONE* **10**, e0135750 (2015).
29. Meng, Q. et al. Protein tyrosine phosphatase receptor type delta (PTPRD) suppresses the expression of PD-L1 in human hepatocellular carcinoma by down-regulating STAT3. *Transl. Cancer Res.* **9**, 5574–5584 (2020).
30. Gide, T. N. et al. Distinct immune cell populations define response to anti-PD-1 monotherapy and anti-PD-1/Anti-CTLA-4 combined therapy. *Cancer Cell* **35**, 238–255.e236 (2019).
31. Casula, M. et al. Germline and somatic mutations in patients with multiple primary melanomas: a next generation sequencing study. *BMC Cancer* **19**, 772 (2019).
32. Pinto, R. et al. The next generation of metastatic melanoma: uncovering the genetic variations for anti-BRAF therapy response. *Oncotarget* **7**, 25135–25149 (2016).
33. Collins, N. B. et al. PI3K activation allows immune evasion by promoting an inhibitory myeloid tumor microenvironment. *J. Immunother. Cancer* **10**, <https://doi.org/10.1136/jitc-2021-003402> (2022).
34. Ng, P. K. et al. Systematic functional annotation of somatic mutations in cancer. *Cancer Cell* **33**, 450–462.e410 (2018).
35. Liu, L. et al. Combination of TMB and CNA stratifies prognostic and predictive responses to immunotherapy across metastatic cancer. *Clin. Cancer Res.* **25**, 7413–7423 (2019).
36. Rozeman, E. A. et al. Survival and biomarker analyses from the OpACIN-neo and OpACIN neoadjuvant immunotherapy trials in stage III melanoma. *Nat. Med.* **27**, 256–263 (2021).
37. Abbott, C. W. et al. Prediction of immunotherapy response in melanoma through combined modeling of neoantigen burden and immune-related resistance mechanisms. *Clin. Cancer Res.* **27**, 4265–4276 (2021).
38. Xie, N. et al. Neoantigens: promising targets for cancer therapy. *Signal Transduct. Target Ther.* **8**, 9 (2023).
39. Alspach, E. et al. MHC-II neoantigens shape tumour immunity and response to immunotherapy. *Nature* **574**, 696–701 (2019).
40. Wang, X. Q. et al. Spatial predictors of immunotherapy response in triple-negative breast cancer. *Nature* **621**, 868–876 (2023).
41. Peri, A. et al. Combined presentation and immunogenicity analysis reveals a recurrent RAS.Q61K neoantigen in melanoma. *J. Clin. Investig.* **131**, <https://doi.org/10.1172/JCI129466> (2021).
42. Immisch, L. et al. Targeting the recurrent Rac1P29S neopeptide in melanoma with heterologous high-affinity T cell receptors. *Front. Immunol.* **14**, 1119498 (2023).
43. Thielmann, C. M. et al. NF1-mutated melanomas reveal distinct clinical characteristics depending on tumour origin and respond favourably to immune checkpoint inhibitors. *Eur. J. Cancer* **159**, 113–124 (2021).
44. Li, Y., Zhao, H., Huang, J., Yan, H. & Zhao, B. The association of ROS1 mutation with cancer immunity and its impact on the efficacy of pan-cancer immunotherapy. *J. Transl. Med.* **22**, 403 (2024).
45. Liu, H. et al. 1057P ROS1 mutation can serve as a potential efficacious predictor of immunotherapy in melanoma patients. *Ann. Oncol.* **32**, S882 (2021).
46. Ma, S. C. et al. De novo mutation in non-tyrosine kinase domain of ROS1 as a potential predictor of immune checkpoint inhibitors in melanoma. *Front Oncol.* **11**, 666145 (2021).
47. Wilmott, J. *Personalised Immunotherapy Platform (PIP-PREDICT) [Clinical Trial: NCT06536257]*, <https://clinicaltrials.gov/study/NCT06536257> (2024).
48. Owsley, J. et al. Prevalence of class I-III BRAF mutations among 114,662 cancer patients in a large genomic database. *Exp. Biol. Med.* **246**, 31–39 (2021).
49. Ng, P. C. & Henikoff, S. SIFT: Predicting amino acid changes that affect protein function. *Nucleic Acids Res.* **31**, 3812–3814 (2003).
50. Chen, S. et al. A genomic mutational constraint map using variation in 76,156 human genomes. *Nature* **625**, 92–100 (2024).
51. Sherry, S. T. et al. dbSNP: the NCBI database of genetic variation. *Nucleic Acids Res.* **29**, 308–311 (2001).
52. Tate, J. G. et al. COSMIC: the catalogue of somatic mutations in cancer. *Nucleic Acids Res.* **47**, D941–D947 (2019).
53. Tamborero, D. et al. Cancer Genome Interpreter annotates the biological and clinical relevance of tumor alterations. *Genome Med.* **10**, 25 (2018).
54. Alexandrov, L. B. et al. The repertoire of mutational signatures in human cancer. *Nature* **578**, 94–101 (2020).
55. Manders, F. et al. MutationalPatterns: the one stop shop for the analysis of mutational processes. *BMC Genom.* **23**, 134 (2022).
56. Austin, P. C. & Stuart, E. A. Moving towards best practice when using inverse probability of treatment weighting (IPTW) using the propensity

- score to estimate causal treatment effects in observational studies. *Stat. Med.* **34**, 3661–3679 (2015).
57. Baek, S., Park, S. H., Won, E., Park, Y. R. & Kim, H. J. Propensity score matching: a conceptual review for radiology researchers. *Korean J. Radio.* **16**, 286–296 (2015).
58. Greifer, N. WeightIt: weighting for covariate balance in observational studies. R package version weightIt v1.1.0, <https://CRAN.R-project.org/package=WeightIt> (2019).
59. Hundal, J. et al. pVAC-Seq: a genome-guided in silico approach to identifying tumor neoantigens. *Genome Med.* **8**, 11 (2016).
60. Reynisson, B., Alvarez, B., Paul, S., Peters, B. & Nielsen, M. NetMHCpan-4.1 and NetMHCIIpan-4.0: improved predictions of MHC antigen presentation by concurrent motif deconvolution and integration of MS MHC eluted ligand data. *Nucleic Acids Res.* **48**, W449–W454 (2020).

## Acknowledgements

This work was supported by Melanoma Institute Australia, the New South Wales Department of Health, NSW Health Pathology, National Health and Medical Research Council of Australia (NHMRC), and Cancer Institute NSW. Including research grants, CINSW Translational Program Grant (TPG 2021/TPG2114). J.S.W. is supported by an NHMRC Fellowship (APP1174325) and Charles Perkins Centre Catchlove-Sylvan MCR Fellowship. T.N.G. is supported by an NHMRC Fellowship and CINSW Fellowship (2020/ECF1244). G.V.L., A.M.M., and R.A.S. are supported by NHMRC Investigator Grants (GNT2007839 and GNT2018514), and G.V.L. is supported by the Melanoma Foundation of the University of Sydney through the University of Sydney Medical Foundation. I.P.S. is supported by a CINSW Early Career Fellowship (ECF1376), NHMRC investigator grant and MRA young investigator award. Support from The Ainsworth Foundation, CLEARbridge Foundation, Melanoma March, The Cameron Family Foundation, Lady Mary Fairfax Charitable Trust, Deborah McMurtrie and John McMurtrie AM, and The Ross Trust, as well as from colleagues at Royal Prince Alfred Hospital and Melanoma Institute Australia, is also gratefully acknowledged. The authors gratefully acknowledge the Australian Genomics Research Facility, Ramaciotti Centre for Genomics and the molecular core facilities of Charles Perkins Centre for the genomic testing. FoundationOne® CDx tests were provided and funded by Roche Products Pty Limited as part of the Match-MEL study (NCT02645149). We would like to thank MIA patients and their families for their contributions to our study.

## Author contributions

Conception and design: Y.M., T.N.G., S.N.L., V. and J.S.W. Acquisition and collection of samples: Y.M., T.N.G., N.G.M., D.V., A.P., E.C.P., H.B., I.P.S., A.M.M., A.B., S.N.L., R.A.S., G.V.L., I.A.V. and J.S.W. Patient Data and Drug Therapy: I.P.S., A.M.M., G.V.L. Analysis and interpretation of data: Y.M., T.N.G., S.N.L., I.A.V. and J.S.W. Review and editing: Y.M., T.N.G., N.G.M., D.V., A.P., E.C.C.-P., P., P., H., B., I.P.S., A.M.M., A.B., S.N.L., R.A.S., G.V.L., I.A.V. and J.S.W. Manuscript preparation and final approval: Y.M., T.N.G., N.G.M., D.V., A.P., E.C.P., H.B., I.P.S., A.M.M., A., B., C.P., P. S.N.L., R.A.S., G.V.L., I.A.V. and J.S.W. Funding: R.A.S., G.V.L., J.S.W.

## Competing interests

G.V. Long has served as a consultant advisor for Agenus, Amgen, Array Biopharma, AstraZeneca, Bayer HealthCare Pharmaceuticals Inc.,

BioNTech SE, Boehringer Ingelheim International GmbH, Bristol Myers Squibb, Evaxion Biotech A/S, GI Innovation Inc., Hexal AG (Sandoz Company), Highlight Therapeutics S.L., IOBiotech, Immunocore Ireland Limited, Innovent Biologics USA Inc., Iovance Biotherapeutics Inc., Merck Sharpe & Dohme, Novartis Pharma AG, OncoSec Medical Australia, PHMR Limited, Pierre Fabre, Regeneron Pharmaceuticals, Scancell Limited, and SkylineDX BV. A.M. R.A. Scolyer has received fees for professional services from MetaOptima Technology Inc., F. Hoffmann-La Roche Ltd., Evaxion, Provectus Biopharmaceuticals Australia, Qbiotics, Novartis, Merck Sharp & Dohme, NeraCare, Amgen Inc., Bristol Myers Squibb, Myriad Genetics, GlaxoSmithKline, SkylineDx BV, and IO Biotech ApS. A.M. Menzies is on the advisory board of BMS, Merck (MSD), Novartis, Roche, Pierre Fabre and Qbiotics. I. Pires da Silva is on the advisory board of Merck Sharp & Dohme; has received fees for professional services from Roche, Bristol Myers Squibb, Merck Sharp & Dohme, Novartis, and Pierre Fabre, Regeneron and Strand; and has had travel support from Bristol Myers Squibb and Merck Sharp & Dohme. M.S. Carlino has served on advisory boards or as a consultant for Amgen, BMS, Eisai, Ideaya, Merck, Sharp & Dohme (MSD), Nektar, Novartis, Oncosec, Pierre-Fabre, Qbiotics, Regeneron, Roche, Merck, Moderna and Sanofi and received honoraria from BMS, MSD and Novartis. All other authors declare no conflicts of interest.

## Additional information

**Supplementary information** The online version contains supplementary material available at <https://doi.org/10.1038/s41698-025-01230-y>.

**Correspondence** and requests for materials should be addressed to James S. Wilmott.

**Reprints and permissions information** is available at <http://www.nature.com/reprints>

**Publisher's note** Springer Nature remains neutral with regard to jurisdictional claims in published maps and institutional affiliations.

**Open Access** This article is licensed under a Creative Commons Attribution-NonCommercial-NoDerivatives 4.0 International License, which permits any non-commercial use, sharing, distribution and reproduction in any medium or format, as long as you give appropriate credit to the original author(s) and the source, provide a link to the Creative Commons licence, and indicate if you modified the licensed material. You do not have permission under this licence to share adapted material derived from this article or parts of it. The images or other third party material in this article are included in the article's Creative Commons licence, unless indicated otherwise in a credit line to the material. If material is not included in the article's Creative Commons licence and your intended use is not permitted by statutory regulation or exceeds the permitted use, you will need to obtain permission directly from the copyright holder. To view a copy of this licence, visit <http://creativecommons.org/licenses/by-nc-nd/4.0/>.

© The Author(s) 2026